Supporting Information for:

Microstructured Air Cavities as High-Index-Contrast Substrates with Strong Diffraction for Light-Emitting Diodes

Yoon-Jong Moon, Daeyoung Moon, Jeonghwan Jang, Jin-Young Na, Jung-Hwan Song, Min-Kyo Seo, Sunghee Kim, Dukkyu Bae, Eun Hyun Park, Yongjo Park, Sun-Kyung Kim, and Euijoon Yoon

This PDF file includes:

Supplementary Figures S1−S10

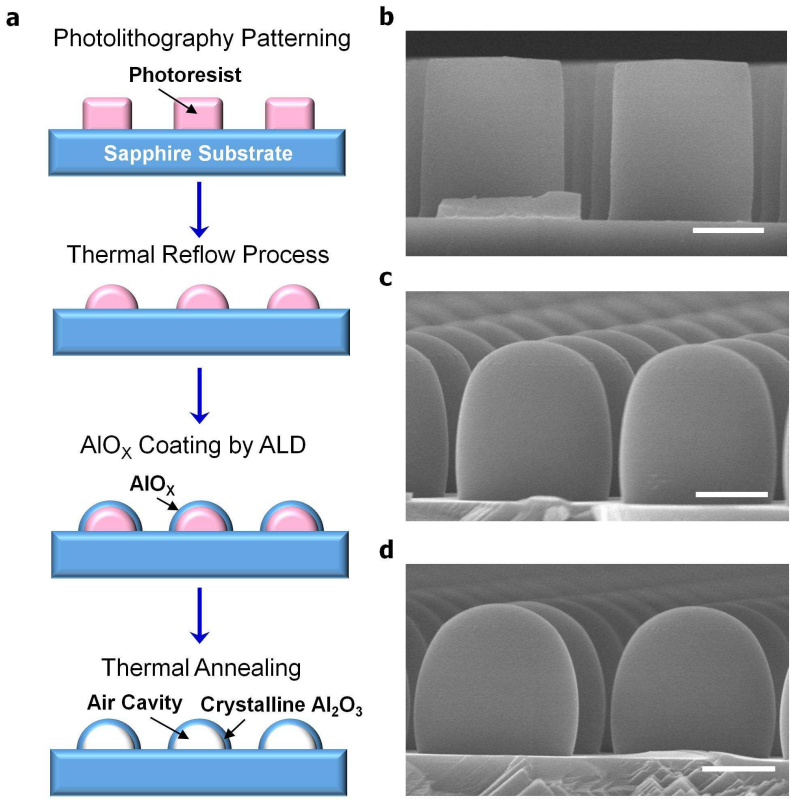

Figure S1. SEM images of thermally treated PR patterns. (a) Fabrication process of the CES template. (b) Cross-section SEM image of an intact PR rod pattern. (c,d) Cross-section SEM images of a cylindrical PR pattern with a thermal reflow process for 40 (panel c) and 50 (panel d) minutes at 150 ˚C: scale bar, 1 μm.

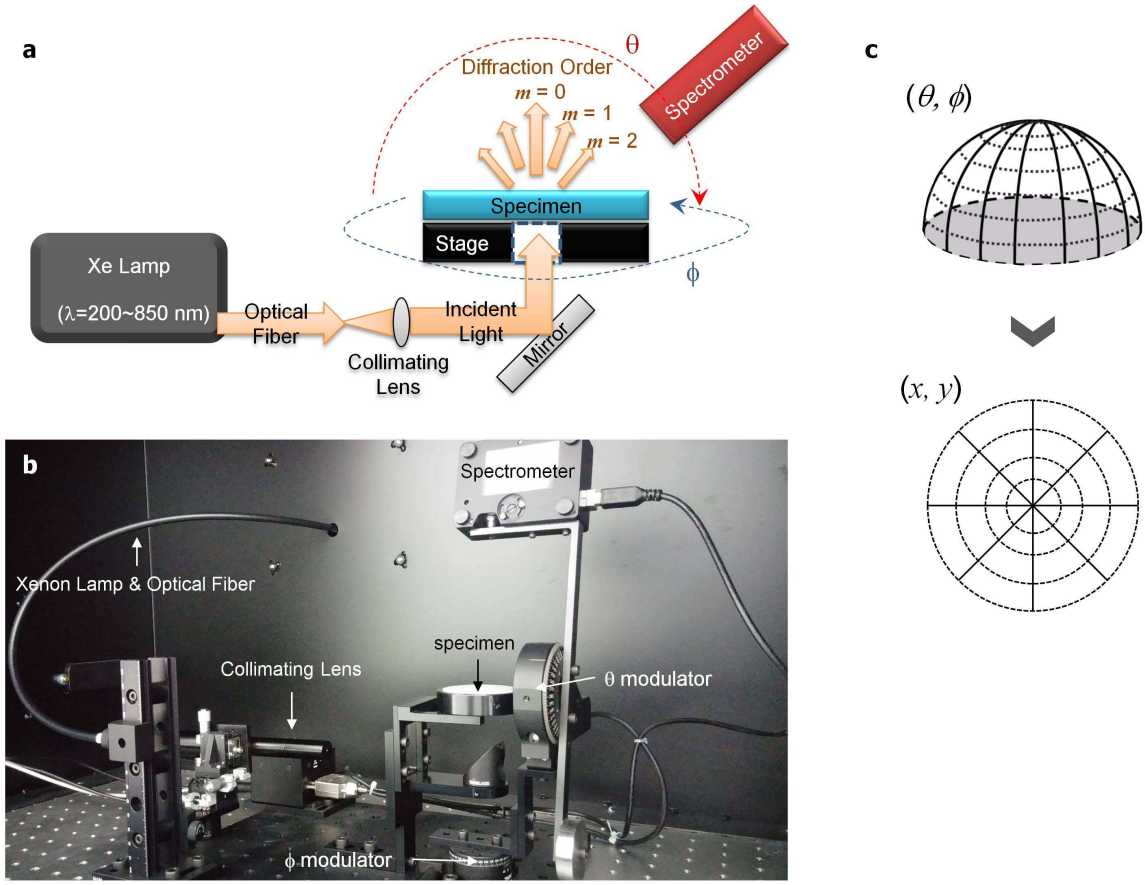

Figure S2. Wavelength-resolved diffraction measurement setup. (a,b) Schematic (panel a) and camera image (panel b) of the home-built wavelength-resolved far-field scanner (c) Schematic illustrating the representation diagram of the measured far-field data.

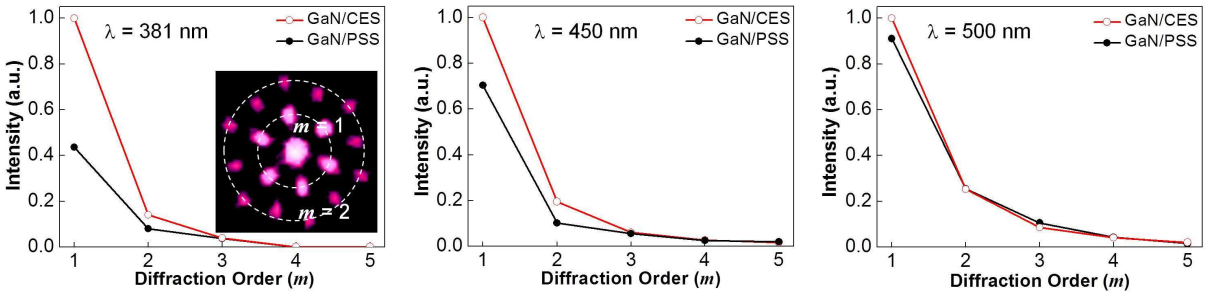

Figure S3. Wavelength-resolved diffraction strength for transmitted light. Diffraction strength versus the diffraction order (m) acquired at λ = 381 (left), 450 (middle), and 500 nm (right) for GaN/CES and GaN/PSS structures. Left inset: representative diffraction image illustrating the diffraction order (m).

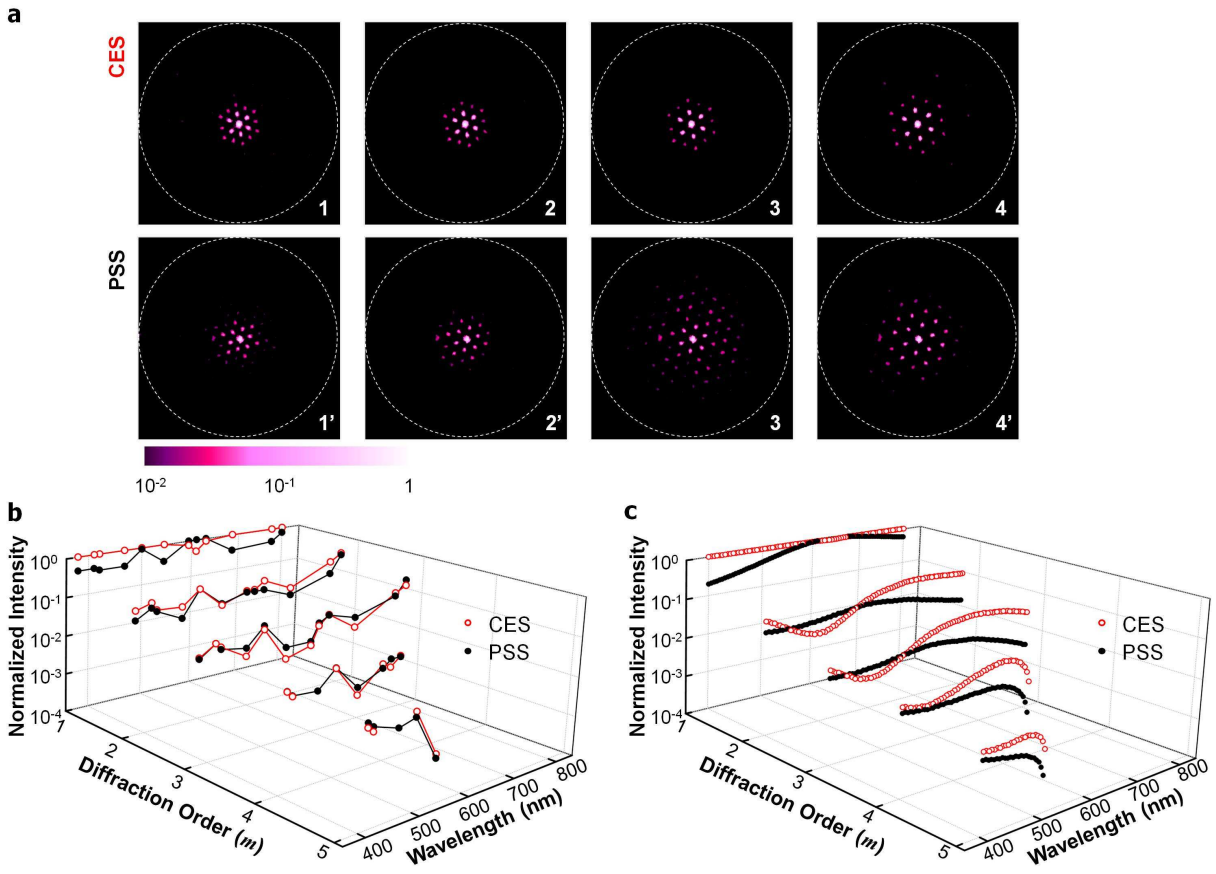

Figure S4. Logarithmic scale of the wavelength-dependent diffraction strength versus the diffraction order. (a) Wavelength-resolved diffraction profiles plotted on a logarithmic scale for GaN/CES and GaN/PSS structures. Labeled profiles correspond to the transmission data labeled identically within Fig. 2a. (b,c) Measured (panel b) and calculated (panel c) logarithmic strength of wavelength-resolved diffraction with respect to the diffraction order (m) for GaN/CES and GaN/PSS structures. For the CES and PSS simulations, hemispherical objects with a radius of 1050 nm were introduced. For the CES object, the inner air cavity was covered with an 80-nm-thick alumina shell.

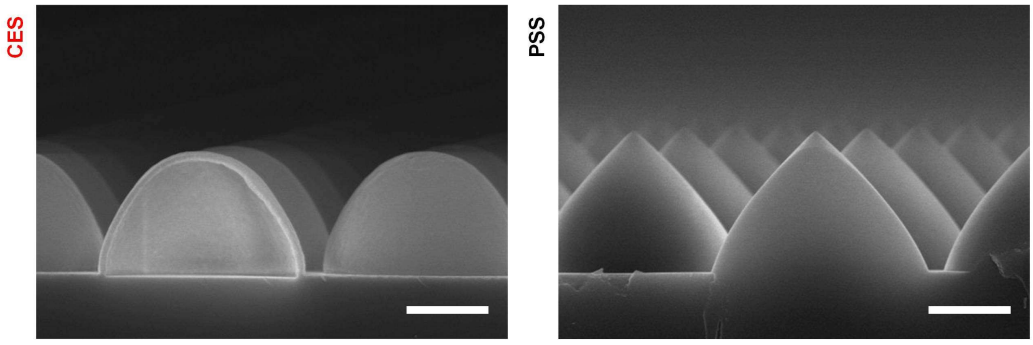

Figure S5. SEM images of CES and PSS growth templates. Cross-section SEM images of the CES (left) and PSS (right) growth templates incorporated into the fabricated LED devices: scale bar, 1 μm.

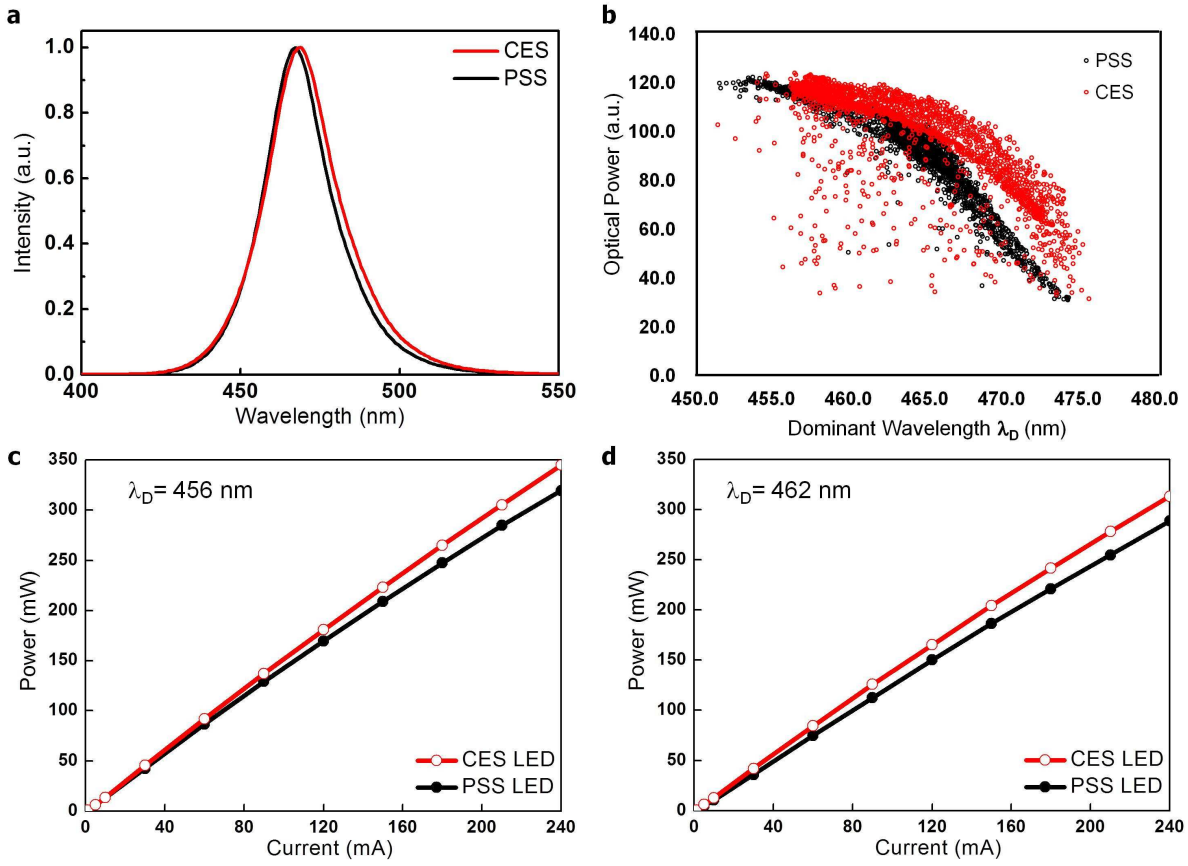

Figure S6. Chip-to-chip variation in the optical power for CES and PSS LED devices with a lateral geometry. (a) Normalized emission spectra from representative the CES and PSS LED devices shown in Fig. 3a. Both devices have the same dominant wavelength of λ = 468 nm. (b) Probe map data for the optical power recorded from wafer-level CES and PSS LED devices. (c,d) Representative optical power-current (*L*-*I*) characteristics of fabricated lateral-geometry CES and PSS LED devices with a dominant wavelength of 456 (panel c) and 462 nm (panel d).

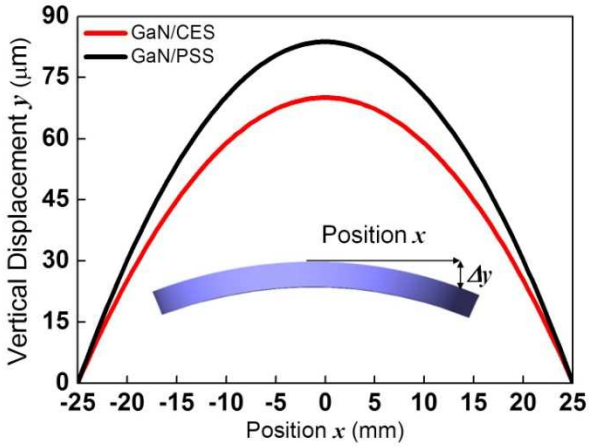

Figure S7. Mechanical stress of GaN/CES and GaN/PSS wafers. Measured center-to-edge vertical displacement for two-inch GaN/CES and GaN/PSS wafers with a 430-μm-thick sapphire substrate.

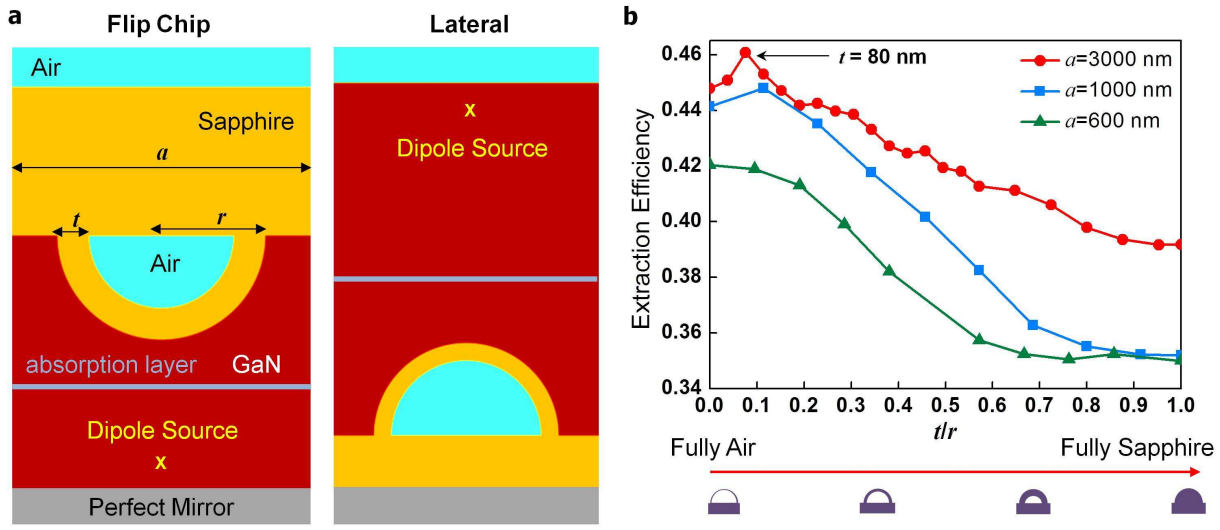

Figure S8. Full-vectorial electromagnetic simulations of the extraction efficiency. (a) Schematics of simulated structures for flip-chip- (left) and lateral-geometry (right) GaN LED structures. Because of a problem related to the computation memory, a 1-μm-thick sapphire substrate was employed for both structures. A 100-nm-thick absorption layer with an extinction coefficient (k) of 0.01 was introduced. (b) Simulated extraction efficiencies of flip-chip-geometry GaN/CES structures ($r = 0.35a$) with various filling fractions of the air cavity for three different pitches: a = 600, 1000, and 3000 nm. For the CES and PSS simulations, hemispherical objects were introduced.

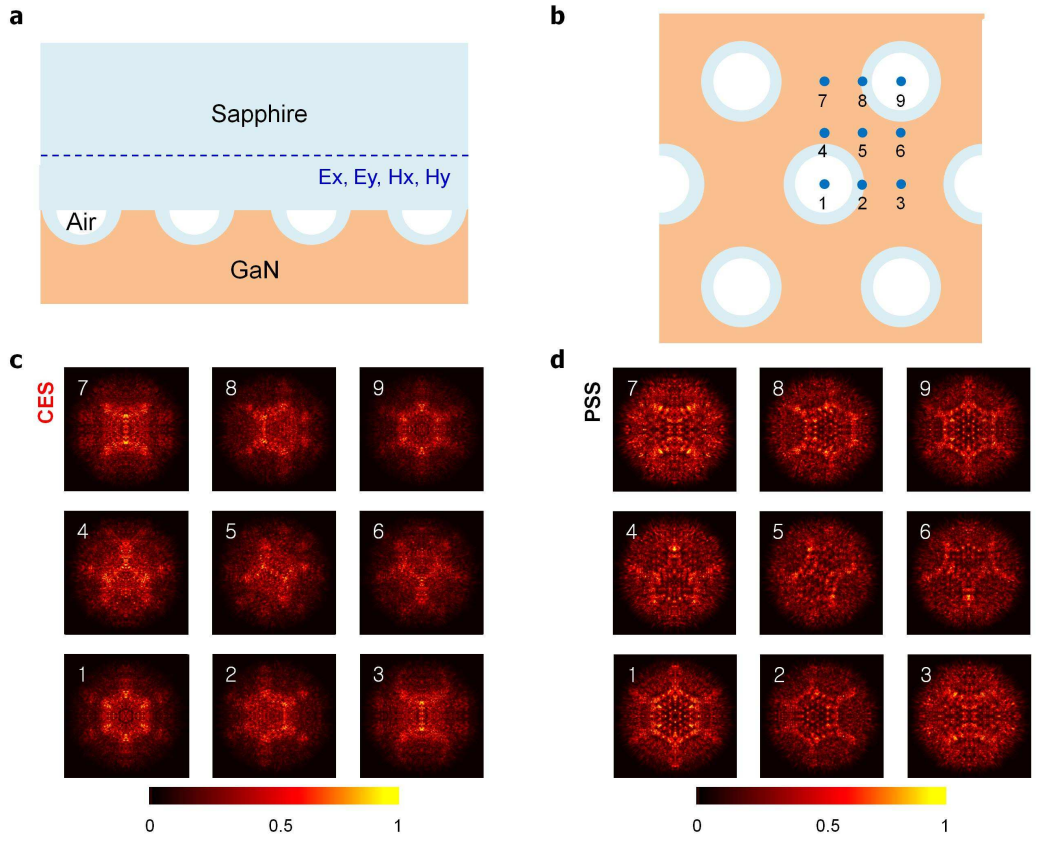

Figure S9. Far-field simulations for GaN LED devices. (a) Schematic of a flip-chip-geometry structure with a patterned substrate. For far-field simulations, in-plane electric and magnetic field profiles were obtained at a certain plane in the sapphire background. (b) Schematic illustrating the relative position of a dipole source within the unit cell. For each position, individual far-field profiles were acquired by near-to-far-field transformation simulations. (c,d) Individual far-field profiles with respect to the position of a dipole source for GaN/CES (panel c) and GaN/PSS (panel d) structures with a pitch of 3000 nm. Monochromatic dipole sources with λ = 450 nm were excited in the GaN medium. For the CES and PSS simulations, hemispherical objects with a radius of 1050 nm were introduced. For the CES, an 80-nm-thick alumina shell was introduced. The labeled far-field profiles correspond to the positions labeled identically within Fig. S9b.

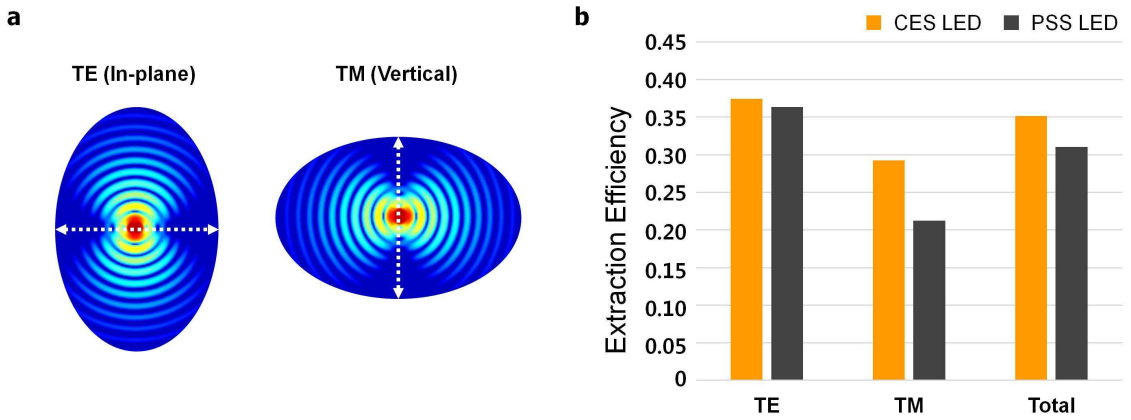

Figure S10. Polarization analysis of the extraction efficiency. (a) Plots of electric field intensities representing the radiation patterns of the dipole sources with transverse electric (TE) and transverse magnetic (TM) polarizations. (b) Extraction efficiencies of flip-chip-geometry CES and PSS LEDs for TE and TM polarized dipole sources which are acquired from the far-field analysis in Figs. 4c and 4d. Total extraction efficiencies were defined by averaging the extraction efficiencies for TE and TM polarizations by taking a weighting factor of 2:1 (TE:TM).